Bimetallic Ni-Cu catalysts for the low-temperature ethanol steam reforming: importance of metal-support interactions

Valentina Nichele[1], Michela Signoretto[1,], Francesco Pinna[1], Elena Ghedini[1], Matteo Compagnoni[2], Ilenia Rossetti[2], Giuseppe Cruciani[3], Alessandro Di Michele[4]*

[1] Molecular Sciences and Nanosystems Dept., Ca' Foscari University, INSTM Unit, Calle Larga Santa Marta 2137, 30123 Venice (Italy).

[2] Chemistry Dept., ISTM-CNR, INSTM Unit, Università degli Studi di Milano, via C. Golgi, 19, 20133 Milan (Italy).

[3] Physics and Earth Sciences Dept., University of Ferrara, via Saragat 1, 44122 Ferrara (Italy).

[4] Physics and Geology Dept., Università degli Studi di Perugia, Via Pascoli, 06123 Perugia (Italy).

**Corresponding author. E-mail: miky@unive.it*

Phone: +39-041-2348650

Fax: +39-041-2348517

Short title: **Bimetallic Ni-Cu catalysts for the low-temperature ethanol steam reforming**

Abstract

The activity of bimetallic Ni-Cu catalysts in ethanol steam reforming was evaluated and compared to the activity of the corresponding monometallic Ni catalyst. Copper addition positively affected the catalytic activity only if the proper metal-support interactions, as well as the proper ratio between the different reducible species, were maintained. This target can be pursued by tuning the synthesis conditions.

Graphical abstract

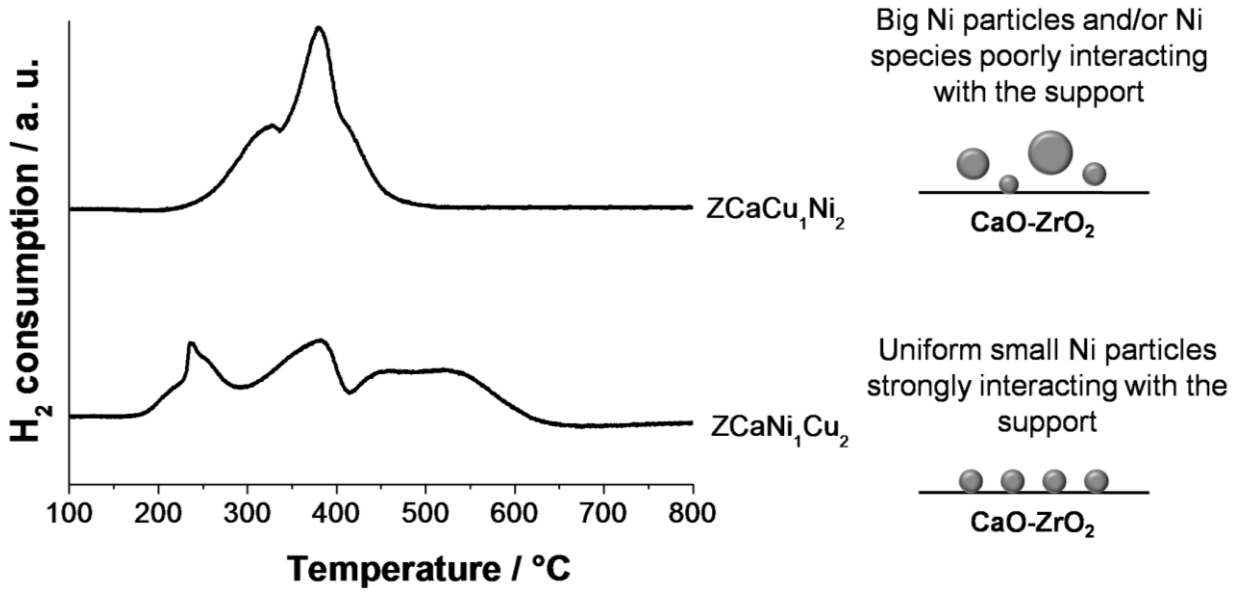

Keywords: Hydrogen; Ethanol Steam Reforming; Ni-Cu catalysts; Synthesis conditions; Metal-support interaction.

1. Introduction

Hydrogen is considered the future energy vector that can meet the ever growing world energy demand in a clean and sustainable way. In order to reduce the dependence from fossil fuels for environmental, economic and political reasons, hydrogen should be produced from renewable sources. Ethanol, which is produced by biomass fermentation and is expected to be available in the near future from second generation biomass, attracted more and more attention as a possible source of hydrogen because it has high hydrogen content, it is renewable, easy to store, handle and transport because of its low volatility and non toxicity.
Hydrogen can be produced by ethanol steam reforming (ESR), an endothermic process which takes place according to the following stoichiometric reaction, Eq.1:

Eq. 1 $$CH_3CH_2OH + 3H_2O \rightleftharpoons 6H_2 + 2CO_2$$

including the water-gas shift of the intermediate CO (Eq. 2), which further increases the hydrogen yield:

Eq. 2 $$CO + H_2O \rightleftharpoons CO_2 + H_2$$

However several reaction pathways can take place; the most important are ethanol dehydrogenation, dehydration or decomposition, that lead to the formation of acetaldehyde, ethylene and methane respectively [1, 2]. The overall process depends on the reaction conditions but also, of course, on the catalyst. Noble metals (Pt, Rh, Ir) show high activity and selectivity in ESR [3-5], but their high cost is a serious drawback. Nickel is as active and selective as noble metals, but it is by far cheaper and more available. Nickel is highly effective in breaking C-C bonds, that is a fundamental requirement for this reaction [6, 7]. Nevertheless, hydrogen yield is usually lowered by the formation of a significant amount of methane [8] if ESR is carried out at conveniently low temperature to limit the heat input to the reactor (*i. e*. 500 °C). Moreover, Ni catalysts may suffer from severe deactivation due to sintering and coking [9-11]. To control sintering phenomena, Ni particles should be stabilized through strong interactions with the support. This is important also to limit coke formation, since it is well established that coking occurs more promptly over large Ni particles and aggregates than over very dispersed Ni crystallites [12-15]. Another possibility is to add a second metal to the Ni-based catalyst. Copper alone is not so efficient for the promotion of ethanol steam reforming because of its low activity in C-C bonds cleavage [16]. Nevertheless, it was reported that copper can segregate the active Ni particles through the formation of Ni-Cu alloys, thus inhibiting both Ni sintering and coking phenomena [8, 17]. Remón et al. [18] reported that the major carbon preventing effect of copper is to block the step sites on nickel particles, preventing the creation of nucleation sites responsible for graphite formation. Moreover, copper addition to nickel enhances the selectivity to hydrogen thanks to the ability of copper to change the affinity for carbon of nickel particles, which inhibits coke formation and improves stability [19, 20]. Copper is considered to increase the selectivity to hydrogen also because of its high activity for water-gas shift reaction [21].
In this work we studied the effect of copper addition to a Ni/ZrO_2 catalyst. We recently found that this catalyst is highly active in ESR [22-25] and that coking, partly related to the presence of Lewis acid sites on the surface of the support, can be efficiently inhibited by doping with a proper amount (9 wt%) of CaO [26]. To further improve the performance of this catalyst, in particular in terms of hydrogen productivity, we decided to modify it by adding copper. The effect of both the calcination temperature and the order of metals addition was evaluated.

2. Experimental Section

2.1 Catalysts preparation

$Zr(OH)_4$ was prepared by a precipitation method [27] at a constant pH of 10. $ZrOCl_2*8H_2O$ (*Sigma-Aldrich, purity ≥ 99.5%*) was dissolved in distilled water and added with a peristaltic pump under vigorous stirring to an ammonia (33%, *Riedel-de Haën*) solution. During the precipitation, the pH value was kept constant at 10.0 ± 0.1 by the continuous addition of a 33% ammonia solution. The hydroxide suspension was aged for 20 h at 90 °C, then filtered and washed with warm distilled water until it was free from chloride ions ($AgNO_3$ test) and finally dried overnight at 110 °C.
Ni, Cu and CaO were added to $Zr(OH)_4$ by means of the incipient wetness impregnation technique using $Ni(NO_3)_2*6H_2O$ (*Sigma-Aldrich, purity ≥ 98.5%*), $Cu(NO_3)_2*3H_2O$ (*Sigma-Aldrich, puriss. p.a.*) and $Ca(NO_3)_2*4H_2O$ (*Fluka, purity ≥ 99%*) as precursors. Ni, Cu and CaO amounts were kept constant (Ni: 10 wt%; Cu: 2 wt%; CaO: 9 wt%).
A reference sample was prepared by adding Ni- and CaO-precursors to $Zr(OH)_4$ simultaneously and calcining at 500 °C for 4 hours in flowing air (50 mL/min STP). This sample is labelled *ZCaNi*.
In order to study the effect of copper addition, Ni-, CaO- and Cu-precursors were simultaneously impregnated on $Zr(OH)_4$. Part of the sample was calcined at 500 °C for 4 hours (*ZCaNiCu*), while the rest was calcined at 800 °C for 4 hours (*ZCaNiCu800*) to verify the effect of calcination temperature.
Two other samples were prepared by adding Ni and Cu in two separate and sequential steps. In *$ZCaNi_1Cu_2$* Ni- and CaO-precursors were added simultaneously to $Zr(OH)_4$, the sample was calcined at 500 °C for 4 hours, then Cu-precursor was added and the catalyst was calcined again at 500 °C for 4 hours. In *$ZCaCu_1Ni_2$* the order of addition of Ni and Cu was the opposite.

2.2 Catalysts characterization

Temperature programmed reduction (TPR) measurements were carried out by placing the catalyst in a quartz reactor and heating in a 5% H_2/Ar mixed gas stream flowing at 40 mL/min at a heating rate of 10 °C/min from 25 to 800 °C. H_2 consumption was monitored by a TCD detector.
X-ray powder diffraction (XRD) patterns were measured by a Bruker D8 Advance diffractometer equipped with a Si(Li) solid state detector (SOL-X) and a sealed tube providing Cu Kα radiation. The samples were reduced in H_2 flow for 1 h at 500 °C (750 °C for ZCaNiCu800) before the analysis. The Rietveld refinement method as implemented in the Bruker TOPAS program was used to obtain the refined unit cell parameters, crystal size, and the quantitative phase analysis (QPA) for the ZrO_2 support and metal phases in the samples. The crystal size determination is achieved by the integral breadth based calculation of volume weighted mean crystallize sizes assuming intermediate crystallite size broadening modelled by a Voigt function. The amorphous fraction was estimated by fixing in the QPA the nickel fraction to the nominal content of 10 wt%. In this way the minimal content of the amorphous phase was calculated. The results of Rietveld refinements are reported in Table 1. Very large uncertainties were obtained for samples containing a poorly crystalline zirconia phase (e.g. ZCaNiCu and $ZCaNi_1Cu_2$). Nevertheless some useful information were obtained even in the presence of an estimated large amorphous fraction.
TEM images have been obtained using a Philips 208 Transmission Electron Microscope. The samples were prepared by putting one drop of an ethanol dispersion of the catalysts on a copper grid pre-coated with a Formvar film and dried in air.
SEM images have been obtained using a Field Emission Gun Electron Scanning Microscopy LEO 1525, after metallization with Cr. Elemental composition was determined using Bruker Quantax EDS.
Micro-Raman sampling was made by an OLYMPUS microscope (model BX40) connected to an ISA Jobin–Yvon model TRIAX320 single monochromator, with a resolution of 1 cm^{-1}. The source

of excitation was a Melles Griot 25LHP925 He-Ne laser that was used in single line excitation mode at l=632.8 nm. The power focused on the samples was always less than 2 mW. The scattered Raman photons were detected by a liquid-nitrogen cooled charge coupled device (CCD, Jobin Yvon mod. Spectrum One).
Temperature programmed oxidation (TPO) of the spent catalysts was carried out by feeding 40 mL/min of a 10 vol% O_2/He gas mixture while heating by 10°C/min from 25 to 650°C.

Table 1. Results from Rietveld refinements of catalysts

Phase	a (Å)	c (Å)	V_{cell} (Å^3)	crystal size (nm)	phase fraction (wt%)
			Sample ZCaNi		
t-ZrO_2	3.622(2)	5.124(7)	67.2(1)	13(1)	89.8(5)
Ni	3.528(2)		43.9(1)	5(1)	10.2(5)
			Sample ZCaNiCu		
t-ZrO_2	3.6(3)	5.1(8)	66(15)	1(7)	82(24) / 57(17)
Ni	3.53(1)		44(1)	3(5)	17(20) / 10**
Cu	3.615*		47.2*	8(2)	3(4) / 2(3)
Amorphous					-- / 31(96)
			Sample ZCaNi$_1$Cu$_2$		
t-ZrO_2	3.63(1)	5.07(1)	67(1)	6(1)	39(3) / 8(1)
Ni	3.533(4)		44.1(2)	5(3)	50(2) / 10**
Cu	3.615*		47.2*	8(1)	10(1) / 2(1)
Amorphous					-- / 80(1)
			Sample ZCaCu$_1$Ni$_2$		
t-ZrO_2	3.624(9)	5.129(3)	67.4(5)	19(2)	70(5) / 24(2)
Ni	3.534(2)		44.1(1)	11(1)	29(4) / 10**
Cu	3.615*		47.2*	8(3)	2(1) / 1(2)
Amorphous					-- / 65(5)
			Sample ZCaNiCu800		
t-ZrO_2	3.623(2)	5.123(5)	67.2(8)	12(1)	90.3(2)
Ni(Cu)	3.5344(3)		44.15(1)	15(1)	9.7(2)

Tab. 1 Results of Rietveld refinement of catalysts.
Notes: t-ZrO_2 stands for 'tetragonal zirconia' (s.g. *P*4$_2$/*nmc*); Ni(Cu) stands for Ni-Cu alloy. Estimated standard deviations in parentheses refer to last significant digit.
*The cell parameter of metal Cu was always close to the tabulated one (PDF card n. 04-0836) and therefore kept fixed to this value.
**Ni fraction was kept fixed to nominal content when refining > 10 wt%. This allowed estimation on the minimal amorphous fraction.

2.3 Catalytic tests: ethanol steam reforming

Activity tests were performed by means of a continuous micropilot plant including an Incoloy 800 downflow reactor (*i.d*. 0.9 cm, length 40 cm) heated by an electric oven connected to an Eurotherm 3204 TIC. The catalysts were pressed, ground and sieved into 0.15-0.25 mm particles and *ca*. 0.5 g were loaded into the reactor after dilution 1:3 (vol/vol) with SiC of the same particle size. The void part of the reactor over and below the catalyst bed has been filled with quartz beads (0.5-1 mm

size). The catalysts were activated in 50 cm^3/min of a 20 vol% H_2/N_2 gas mixture, while heating by 10 °C/min up to 500 °C (750 °C for ZCaNiCu800), then kept for 1 h. During activity testing 0.017 cm^3/min of a 3:1 (mol/mol) H_2O:CH_3CH_2OH liquid mixture were fed to the reactor by means of a Hitachi, mod. L7100, HPLC pump. 56 cm^3/min of N_2, used as internal standard, and 174 cm^3/min of He were also added. Such dilution of the feed stream was calibrated so to keep the reactants mixture in the vapour phase even at zero conversion at the reactor outlet. This allows the direct quantification of all the reactants and products in a single step, with more reliable quantification of carbon balance, conversion and selectivity. Internal and external mass transfer limitations were found negligible during system set up, given the high linear velocity of the gas mixture and the selected particle size.
The activity tests were carried out at atmospheric pressure, GHSV = 2500 h^{-1} (referred to the ethanol + water gaseous mixture) at 500 °C for the samples calcined at 500 °C, at 750 and 500 °C for the sample calcined at 800 °C.
The analysis of the out-flowing gas was carried out by a gaschromatograph (Agilent, mod. 7980) equipped with two columns connected in series (MS and Poraplot Q) with a thermal conductivity detector (TCD), properly calibrated for the detection of ethanol, acetaldehyde, acetic acid, acetone, water, ethylene, CH_4, CO, CO_2, H_2. Material balance on C-containing products was checked to quantify coke deposition. Repeated analyses of the effluent gas were carried out every hour and the whole duration of every test was *ca*. 8 h. The raw data, expressed as mol/min of each species outflowing from the reactor, have been elaborated as detailed in Ref. 23 and 25.

3. Results and discussion

3.1 Effect of copper addition

In Table 2 the results of ESR tests are reported. Data reported are averaged out 4-8 h-on-stream.

	Blank test	**ZCaNi**	**ZCaNiCu**	**$ZCaNi_1Cu_2$**	**$ZCaCu_1Ni_2$**	**ZCaNiCu800**	**ZCaNiCu800 750 °C**
EtOH conversion / %	13 ± 5	100 ± 0	72 ± 9	100 ± 0	100 ± 0	48 ± 11	100 ± 0
H_2O conversion / %		63 ± 5	47 ± 2	68 ± 2	52 ± 6	47 ± 6	60 ± 2
H_2 productivity / mol / min kg_{cat}	-	0.86 ± 0.05	0.45 ± 0.10	1.04 ± 0.04	0.65 ± 0.08	-	1.13 ± 0.02
CH_4 selectivity / %	-	13 ± 1	5 ± 1	12 ± 2	4 ± 1	11 ± 2	-
CH_3CHO selectivity / %	-	-	36 ± 4	-	7 ± 3	38 ± 9	-
C_2H_4 selectivity / %	-	-	19 ± 5	2 ± 2	14 ± 3	19 ± 2	-

Tab. 2: Results of the activity tests for ethanol steam reforming at 500 °C (in the last column, at 750 °C for ZCaNiCu800). Activation at 500 °C for 1 h for every sample except ZCaNiCu800, activated at 750 °C for 1 h. Time-on-stream: 8 h, data averaged out 4-8 h-on-stream.

By analyzing the results related to ZCaNiCu it is possible to evaluate the effect of copper addition, with respect to the activity of the reference sample ZCaNi. Contrary to what expected, Cu doping has made the catalytic performance worse. Ethanol conversion is much lower with ZCaNiCu than with ZCaNi. In particular, ethanol conversion is complete and stable with ZCaNi (Fig. 1(a)), while

in the case of ZCaNiCu it decreases sharply after about 3 h-on-stream, in correspondence to an increase of the carbon balance (Fig. 1(b)).

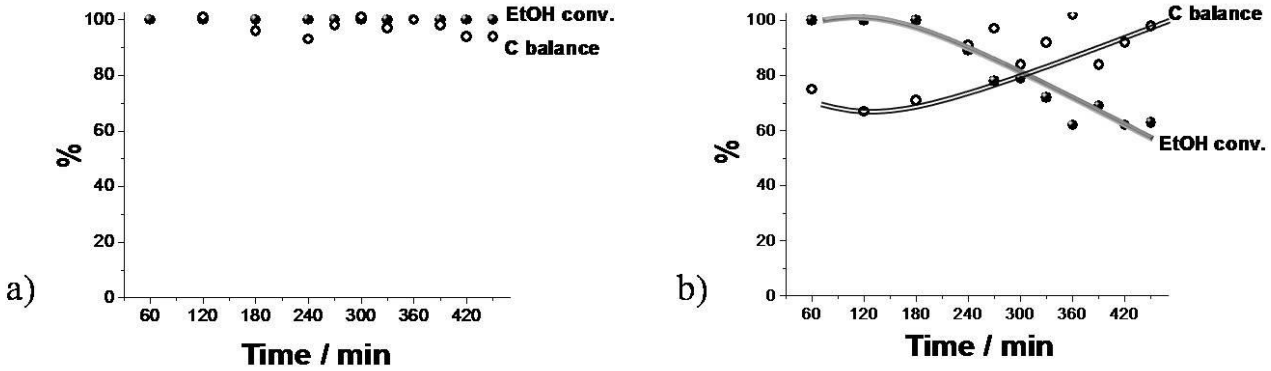

Fig. 1: Ethanol conversion (●) and C balance (**o**) trends for: a) ZCaNi; b) ZCaNiCu.

Contemporarily, the selectivity to acetaldehyde and ethylene, initially nil, started increasing after *ca*. 3 h-on-stream, reaching the steady state value reported in Table 2. Although it may be correlated to many factors, *i. e*. the formation of different species, the carbon balance can be conveniently taken as index of possible catalyst coking. In particular, low values of C balance can denote coke formation. In the case of ZCaNiCu, the low C balance (average value: 69%) in the first three hours of the test seems to suggest that a certain accumulation of coke took place (*vide infra*), leading to deactivation of the catalyst and a fast decrease of ethanol conversion and increase in the selectivity of by-products.

This result can be related to the fact that ZCaNiCu shows a certain selectivity to C2 by-products, that were absent with ZCaNi. The presence of these by-products can be ascribed to copper, which is not active in C-C bonds cleavage, as already reported in the Introduction (section 1). It seems that the presence of copper favoured mainly the secondary reactions leading to by-products, such as acetaldehyde and ethylene, which are precursors of coke. The formation of coke, suggested by the initial low C balance, led to the deactivation of the Ni active sites of the catalyst, indicated by the decrease of ethanol conversion. As a consequence of the formation of significant amounts of by-products, a strong decrease of hydrogen productivity was also observed.

In conclusion, copper addition was not satisfactory for ESR. Several characterization measurements were carried out in order to explain these results.

The TPR profiles of ZCaNi and ZCaNiCu are reported in Fig. 2.

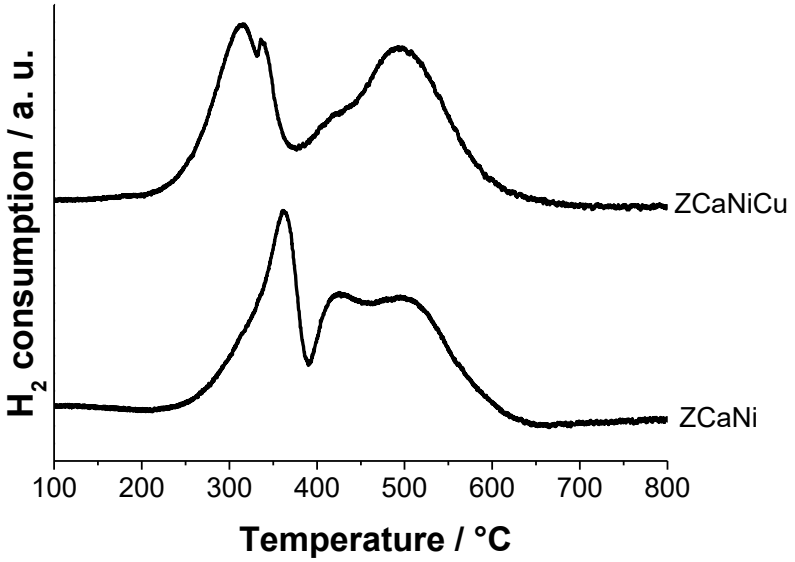

Fig. 2: TPR profiles of ZCaNi and ZCaNiCu.

For both samples several reduction peaks, in a broad region between 250 and 550 °C, can be detected. As for ZCaNi, since it is known that Ni^{2+} is reduced to Ni^0 without any intermediate oxide [28], the presence of several peaks suggests the existence of NiO species differently interacting with the support [22, 29]. The first peak at 360 °C can be assigned to poorly interacting NiO, which is more easily reducible, since unsupported NiO reduces at about 280 °C [30, 31]. The second and third peaks, at about 420 °C and 510 °C, respectively, can be ascribed to NiO progressively more strongly interacting with the support [32, 33]. No peak related to the reduction of Ca^{2+} can be detected, but CaO modifies nickel reducibility. As we previously reported [26] and according to the literature [29, 34], in ZCaNi Ca^{2+} replaces Zr^{4+} in the lattice, thus generating oxygen vacancies which weaken the Ni-O bond and increase nickel reducibility (*i. e.* the intensity of the first peak) with respect to the undoped sample.
With regard to ZCaNiCu, the same three peaks related to Ni^{2+} reduction can be noticed, plus one peak at 280 °C ascribable to the reduction of CuO. A lower reduction temperature can be ascribed to lower metal-support interaction strength and/or to bigger particle size of NiO. Nevertheless, a substantial difference in the relative intensity of the three Ni peaks must be underlined, that is the increase of the intensity of the third peak (the fraction of NiO with strong interactions with zirconia) at the expense of the first two (NiO weakly and non-interacting). Even if the TPR analysis is not used here as a quantitative technique, the intensity of a peak is roughly proportional to the amount of reduced species. We can conclude that copper addition seems to have increased the fraction of strongly interacting Ni species. In our previous works [22-25] we demonstrated that the interactions between the active phase and the support play a key role in determining the performance of a catalysts. However, it also appears a non negligible contribution of highly reducible Ni species. TEM characterization (Fig. 3) helps throwing light on the attribution of these reduction features.

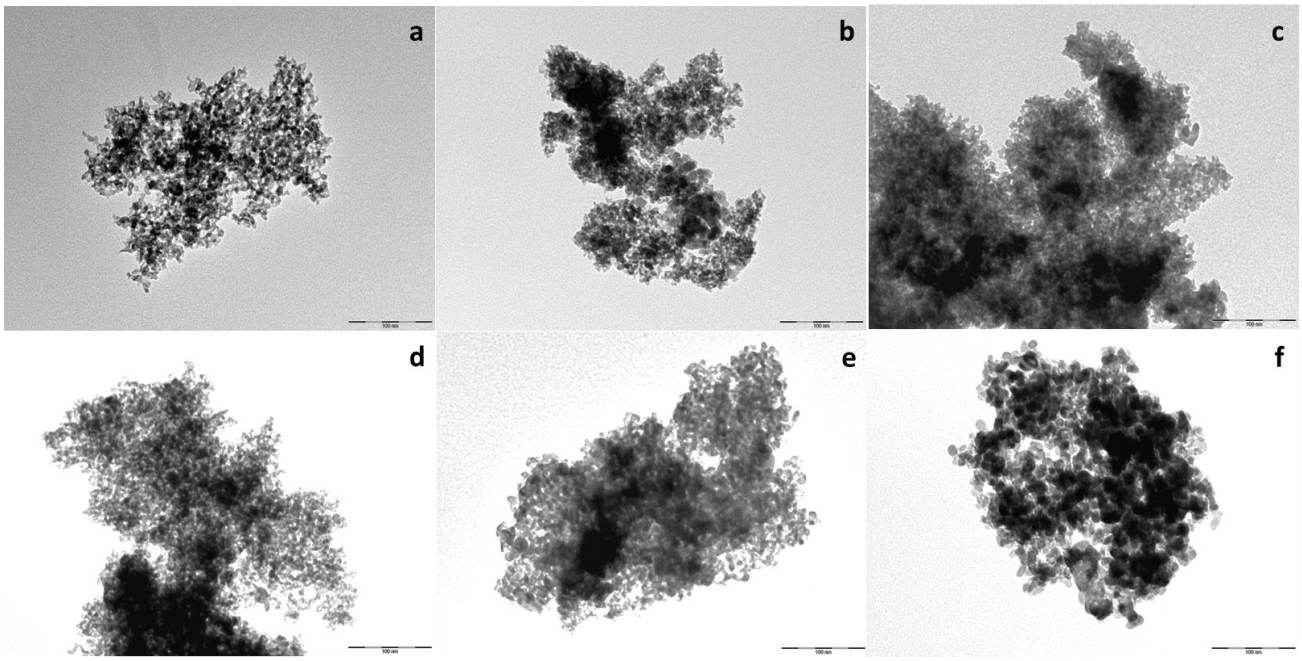

Fig. 3: TEM micrographs of fresh catalysts. a) ZCaNi; b-c) ZCaNiCu; d) $ZCaNi_1Cu_2$; e) $ZCaCu_1Ni_2$; f) ZCaNiCu800. Marker size 100 nm.

The fresh ZCaNi sample (Fig. 6.3(a)) is characterized by a uniform array of 5-10 nm Ni particles, whereas sample ZCaNiCu (Fig. 6.3(b)) is constituted by poorly uniform metal particles, where much bigger particles coexist with smaller ones. This confirms the attribution of the low temperature TPR peak to sintered Ni particles.
The results here reported seem to suggest that also the ratio between the different reducible species is important and correlated with metal particle size.
For a further understanding of the role of crystallographic nature of metal/support phases on the catalytic performances, XRD patterns of ZCaNi and ZCaNiCu were taken as reported in Fig. 4.

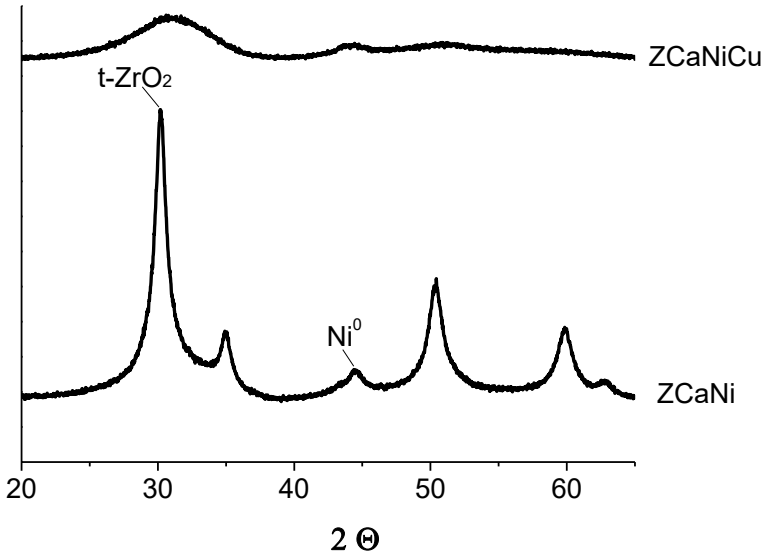

Fig. 4: XRD powder patterns of reduced ZCaNi and ZCaNiCu.

As for ZCaNi, zirconia is present only in the tetragonal phase (the most intense peak at $2\theta \approx 30°$). In our previous study [26] we showed that Zr^{4+} substitution by Ca^{2+} takes place; this replacement

does not affect the nature of the ZrO_2 polymorph of the support, but it modifies Ni reducibility, in accordance with the TPR results, because oxygen vacancies are generated. Nickel appears only in the metallic form (peak at $2\theta = 44.5°$), suggesting that the reduction treatment at 500 °C substantially reduced all Ni^{2+} to Ni^0.
With regard to ZCaNiCu, a substantial difference can be detected: zirconia in this sample appears very poorly crystalline and a very small crystal size were obtained from Rietveld refinement for the Ni and Cu crystallites . This could be due to the synthetic approach we adopted, in which all metals have been added to the support simultaneously. It is known that dopant addition can modify the crystallization process [35, 36].
In conclusion, besides the different ratio between the NiO species on the support, another important difference between ZCaNi and ZCaNiCu can be highlighted, that is the crystallographic nature of zirconia, which is crystalline in ZCaNi, while it is very poorly crystalline in ZCaNiCu.
Since the catalytic behaviour of the two samples is completely different, we decided to check the role of both the ratio between the various NiO species on the support and the crystallographic nature of zirconia. To do this, one possible way is to modify the synthesis procedure.

3.2 Effect of the order of metals addition

The results have shown that the contemporary addition of all the metals alters the crystallization process, so we decided to add Ni and Cu in two separate and sequential steps (samples $ZCaNi_1Cu_2$ and $ZCaCu_1Ni_2$ described in Section 2.1). The catalytic results reported in Table 2 show that the two samples have markedly different catalytic performance, also if compared to the reference catalyst ZCaNi, confirming that the synthesis procedure can strongly affect the catalytic behaviour.
In particular, we can observe that ethanol conversion is complete with both $ZCaNi_1Cu_2$ and $ZCaCu_1Ni_2$, but the products distribution is totally different once again.
With regard to $ZCaCu_1Ni_2$, the products distribution is quite similar to the ZCaNiCu one. A certain amount of C2 by-products and a low H_2 productivity can be achieved. As with ZCaNiCu, also in this case the presence of copper seems to negatively affect the conversion of by-products, acetaldehyde and ethylene, which are not completely converted over the active phase. However, the observed selectivity to acetaldehyde and ethylene is lower when Cu is added before Ni with respect to their contemporary addition. Accordingly, the selectivity to ethylene and acetaldehyde, initially nil, started increasing after 4 h-on-stream to the steady state value reported in Table 2. Thus we can conclude that the addition of Cu modifies the Ni active sites, partially limiting their activity in C-C bond cleavage, depending likely on its surface exposure.
On the contrary, the behavior of $ZCaNi_1Cu_2$ is in line with that of ZCaNi, but the ESR results are even better. In fact, all other results being equal, hydrogen productivity increased from 0.86 (reference ZCaNi) to 1.04 mol/min kg_{cat}. This result is accompanied by a higher water conversion with $ZCaNi_1Cu_2$ and the absence of C2 by-products (with the exception of a very little formation of ethylene towards the end of the test).
Some characterization measurements have been carried out to interpret these results.
The XRD patterns of $ZCaNi_1Cu_2$ and $ZCaCu_1Ni_2$ are reported in Fig. 5 and compared with ZCaNi.

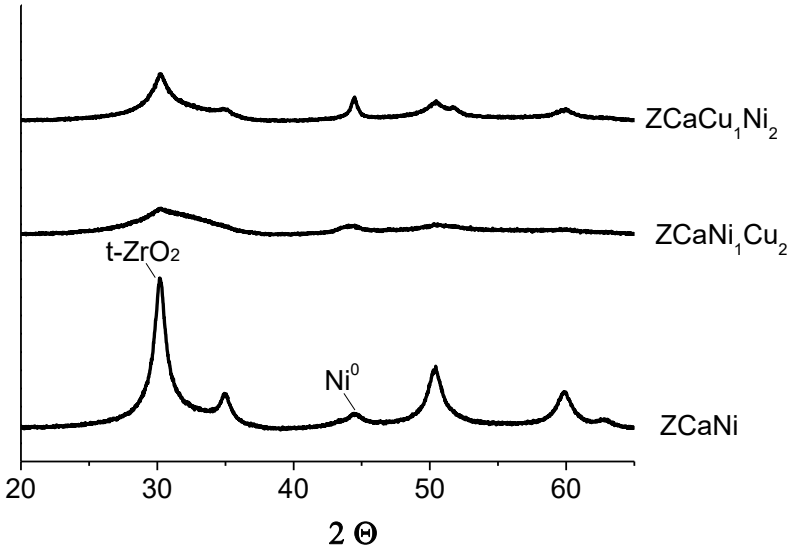

Fig. 5: XRD powder patterns of reduced ZCaNi, $ZCaNi_1Cu_2$ and $ZCaCu_1Ni_2$.

Looking at these patterns along with data in Table 1 it can be noted that both $ZCaNi_1Cu_2$ and $ZCaCu_1Ni_2$ samples contain a major fraction of amorphous zirconia phase. This causes an intensity bump which is responsible for the high angle asymmetry of the most intense zirconia peak. The refined crystal size for t-ZrO_2 in $ZCaCu_1Ni_2$ (see Tab. 1) is relatively large suggesting that a minor component of better crystallized zirconia coexists with the amorphous phase. Concerning the Ni and Cu metal phases, while the peak at about about 44° 2θ is broad in sample $ZCaNi_1Cu_2$ and can be interpreted as the partial overlap of separate Ni and Cu peaks, in the case of $ZCaCu_1Ni_2$ this interpretation is less straightforward because the appearance is that of a relatively sharp single peak corresponding to relatively large Ni nanocrystals. On this basis and given the very low refined fraction of Cu, the occurrence of a Ni-Cu alloy cannot be ruled out altogether. The refined larger cell parameter of Ni does not provide a clear-cut indication because of the large standard errors (see Tab. 1).

The large amorphous content in $ZCaNi_1Cu_2$ and $ZCaCu_1Ni_2$ samples seem to confirm that the addition of both metals hampers the crystallization of the catalyst. On the other hand, the crystalline phase of the support does not affect the catalytic activity so deeply, since good catalytic performance was achieved with the almost amorphous $ZCaNi_1Cu_2$ sample.

With regard to the second parameter we decided to investigate, namely the ratio between the different NiO species on the support, the TPR profiles of the samples are reported in Fig. 6.

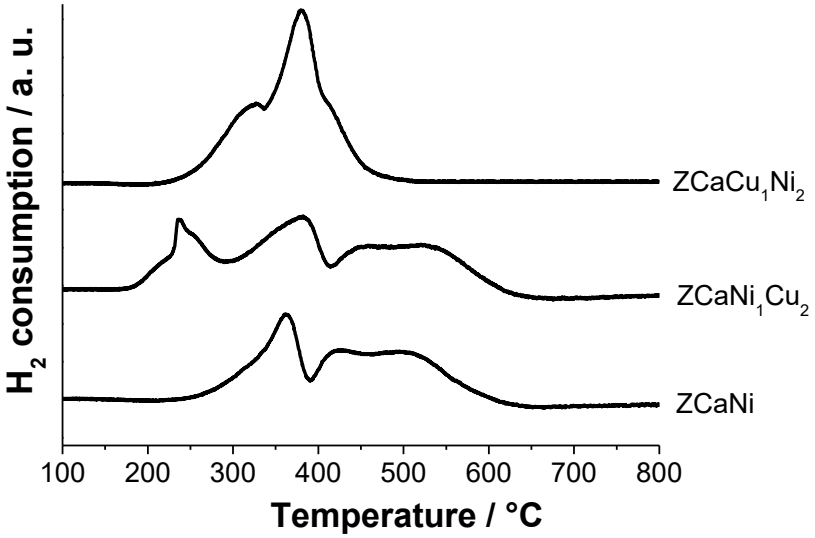

Fig. 6: TPR profiles of ZCaNi, $ZCaNi_1Cu_2$ and $ZCaCu_1Ni_2$.

Comparing the TPR pattern of $ZCaNi_1Cu_2$ with the ZCaNi one, it can be noticed that in $ZCaNi_1Cu_2$ a CuO species reduction peak is located between 180 and 290 °C. With regard to the region of Ni^{2+} reduction, the two profiles are almost identical, in terms of both the position of the peaks and their relative intensities. On the contrary, the TPR profile of $ZCaCu_1Ni_2$ is completely different. The most evident differences lies in: i) the final reduction temperature of NiO, which was lower of about 200 °C (from 650 to 450 °C); ii) the relative distribution of the various Ni^{2+} species. In the literature it is often reported that the presence of copper lowers the reduction temperature of nickel [20, 37, 38]. Pérez-Hernández et al. [39], for example, reported that Cu probably causes spillover of hydrogen on nickel, inducing a competitive reduction of both copper oxide and NiO. Our results show that this depends also on the synthesis approach. The sequential impregnation of Ni and Cu precursors ($ZCaNi_1Cu_2$ and $ZCaCu_1Ni_2$) leads to better results than the simultaneous one (ZCaNiCu). Nevertheless the order of metals impregnation is important as well, as reported also by other authors [40, 41]. In our case, the catalytic results showed that $ZCaNi_1Cu_2$ is more active than $ZCaCu_1Ni_2$. Maybe this can be ascribed to the fact that in this sample the proper ratio between NiO species with medium and strong interactions with the support has been preserved, as in the reference sample ZCaNi. On the contrary, in $ZCaCu_1Ni_2$ NiO with low interaction seems to be present.
TEM analysis is reported in Fig. 3 also for these samples. Substantially uniform, ca. 5 nm, metal nanoparticles may be observed for sample $ZCaNi_1Cu_2$, whereas a broader particle size distribution was evident for sample $ZCaCu_1Ni_2$.
By considering all these results we may conclude that the composition and synthesis conditions which allow the formation of stable and uniform small Ni particles, as in the case of samples ZCaNi and $ZCaNi_1Cu_2$, lead to high activity and stability of the catalyst with time-on-stream. The absence or limited formation of coke deposits ensures the absence of C2 by-products. The latter are usually found when Ni becomes more and more covered by coke, which effectively limits the C-C bond breaking ability of the active site. This is likely due to the progressively lower availability of vicinal Ni sites for C-C bond cleavage. Therefore, when big Ni particle size is present and/or Ni species poorly interacting with the support which easily sinter during use, a low initial C balance is usually observed at the beginning of the test, increasing with time-on-stream accompanied by a decrease in ethanol conversion and increasing selectivity towards ethylene and acetaldehyde.

3.3 Effect of the calcination temperature

Calcination temperature is another important parameter that can affect both the interactions between metal and support and the crystallographic phase of the support. We recently showed that the calcination temperature affects the speciation of Ni when supported over oxides which establish a strong metal support interaction [42, 43]. For instance, when Ni/TiO_2 is calcined at 500 °C it is completely inactive, whereas when calcined at 800 °C it exhibits satisfactory catalytic performance. In the present case a different calcination temperature may also affect the mutual interaction between the two metals. Therefore, a sample for comparison has been prepared by contemporarily adding Ni and Cu precursors and calcining at 800 °C (sample ZCaNiCu800). This sample was tested at 500 °C after activation at 750 °C under reducing conditions (Tab. 2). A further test at 750 °C was also added.

The catalytic performance of sample ZCaNiCu800 at 500 °C was even worse than that achieved after calcination at 500 °C, with negligible H_2 productivity and lower activity for both ethanol and methane reforming. Selectivity to C2 by-products and the decrease of ethanol conversion became evident after the first hour-on stream. It has been also observed that C balance was rather low at the beginning of the test (ca. 86%) and increased with time-on-stream to reach ca. 100%. This behavior may be related to some sintering of the active phase with respect to the sample calcined at 500 °C, inducing broader formation of carbon filaments which induce a faster catalyst deactivation. By contrast, operation at 750 °C gave rise to satisfactory and stable results, with full ethanol conversion and good carbon balance, no C2 by-products and no methane. This means that at high temperature coke gasification occurs and avoids the encapsulation of the active phase which leads to the deactivation observed at 500 °C.

Upon calcination of ZCaNiCu catalyst at 800 °C a clear shift to lower 2-theta angle (larger *d*-spacing) is observed for the diffraction line of metal (see XRD patterns in Fig. 7).

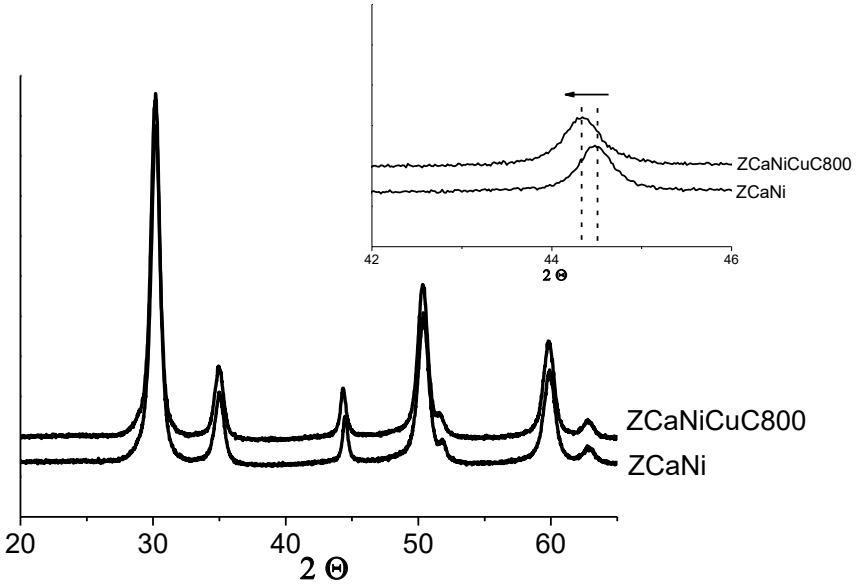

Fig. 7: XRD patterns of ZCaNi and ZCaNiCu800.

Due to the increased crystallinity of sample upon calcinations at 800°C the Rietveld refined unit cell parameter is affected by a small error (see Tab. 1) and is intermediate between that of pure Ni and pure Cu, showing that a Ni-Cu alloy was formed. Furthermore, the TPR analysis (not reported for the sake of brevity) evidenced a much higher reducibility of Ni in sample ZCaNiCu800 with respect to sample ZCaNi. In particular, only highly reducible Ni species survived and the more disperse ones, strongly interacting with the support, completely disappeared. This confirms the tendency to sinter of Ni, according to our previous results [23, 24, 42], and helps elucidating why at 500 °C, where coke gasification is not useful to clean up metal surface, progressive and fast deactivation takes place.

Therefore, preparation conditions which favor the instauration of a stronger metal support interaction allow to keep dispersed the active phase and limit the formation of coke filaments during low temperature operation. The relative amount of these species may be correlated with catalyst life during testing at 500 °C. Indeed the sample for which only very reducible species were present was the least stable. By contrast, samples characterized by a significant concentration of less reducible Ni species (higher dispersion and stronger metal-support interaction) demonstrated higher activity for ethanol (and methane) reforming and above all higher stability with time-on-stream. This is ultimately due to a higher resistance towards coking.

3.4 Spent samples

Finally, the spent samples have been characterized by TEM (Fig. 8), FE-SEM and Raman spectroscopy (Fig. 9).

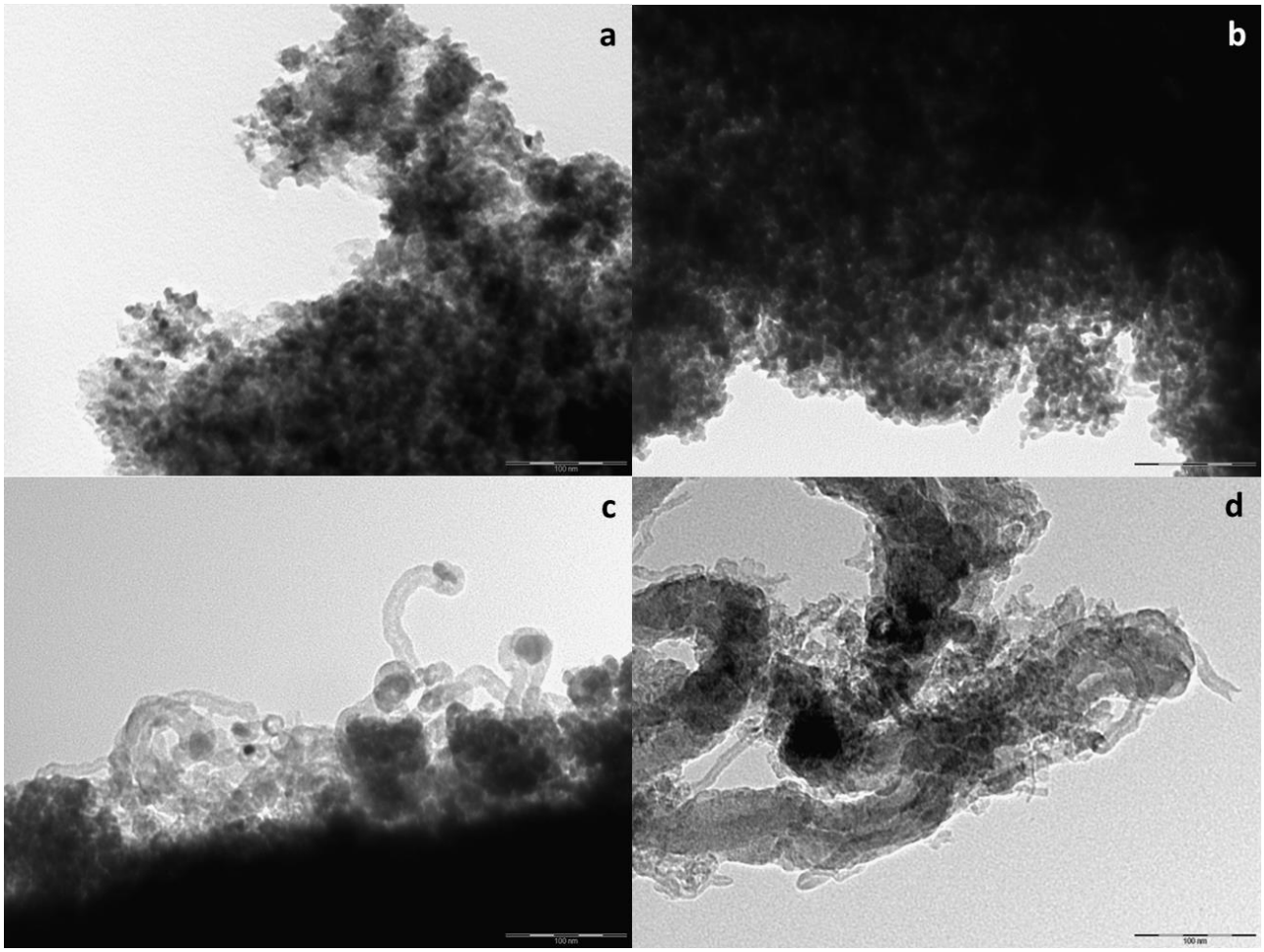

Fig. 8: TEM images of spent samples. a) $ZCaNi_1Cu_2$; b-c) ZCaNiCu; d) ZCaNiCu800. Marker size 100 nm.

TEM confirms limited sintering after use of samples ZCaNiCu and $ZCaNi_1Cu_2$. This confirms that the presence of poorly reducible species, *i. e.* strongly interacting with the support, helps in keeping Ni dispersed during use. Some formation of carbon nanotubes is observed for ZCaNiCu and substantially due to bigger metal particles, which are well known to be more prone to C accumulation (Fig. 8c). According to the much bigger Ni particle size, extensive nanotubes formation was achieved with sample ZCaNiCu800 (Fig. 8d). In all cases the formed C nanotubes showed a multiwalled structure with external diameter of 28-29 nm. Some graphitic C deposition

may also be present due to the presence of some residual Lewis acid sites on the ZrO_2 support, as evidenced by micro-Raman analysis (Fig. 9).

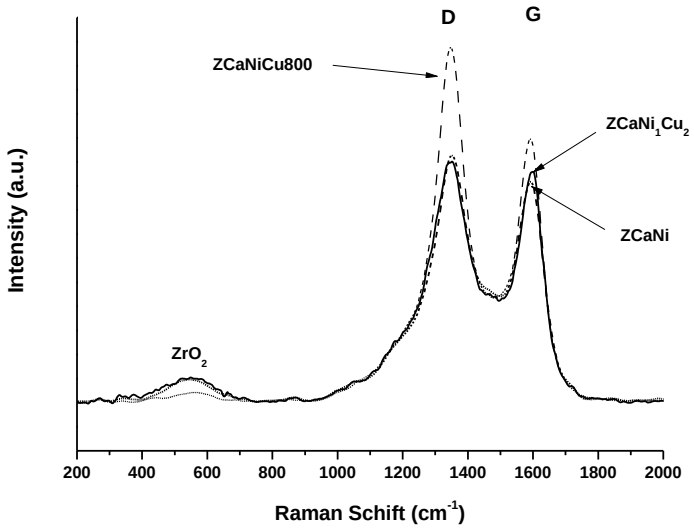

Fig. 9: MicroRaman spectra of spent samples.

The latter spectroscopy allows to identify two typical bands ascribable to coke, the D and G contributions. The latter is usually attributed to ordered graphite layers, whereas the former is mostly attributed to much disordered carbon species with respect to graphite layers (amorphous carbon and nanotubes) and is predominant for sample ZCaNiCu800.
TPO analyses were also carried out on the spent samples. They may further help elucidating the nature of carbon species deposed on the samples, since lower oxidation temperature (T_{ox}) may be attributed to amorphous carbon, whereas more ordered forms such as nanotubes and graphitic layers are expected to oxidise at higher temperature. According to this qualitative scale, the coke deposed over sample ZCaNiCu, with T_{ox} <450 °C, was predominantly amorphous. T_{ox} progressively increased with $ZCaNi_1Cu_2$ and $ZCaCu_1Ni_2$ and finally a very intense peak with maximum at 589 °C characterised sample ZCaNiCu800, which was abundantly covered by carbon nanotubes.

4. Conclusions

The activity of bimetallic Ni-Cu catalysts supported on a CaO-doped zirconia in ethanol steam reforming was evaluated and compared to the activity of the corresponding monometallic Ni catalyst. The results showed that big Ni particles and/or Ni species poorly interacting with the support, which easily sinter during use, cause a low initial C balance, accompanied by a decrease in ethanol conversion and an increase in selectivity towards C2 by-products.
High activity and stability of the catalyst were reached by properly tuning the synthesis conditions in order to obtain the formation of stable and uniform small Ni particles (*i. e.* favoring the instauration of a stronger metal support interaction). The separate and sequential addition of the metals, as well as the proper calcination temperature, are compulsory to achieve the best performance.

Acknowledgements

The authors are indebted to Carlotta Pagan for the excellent technical assistance. Valentina Nichele acknowledges MIUR for her PhD scholarship.

References

[1] Benito M, Sanz JL, Isabel R, Padilla R, Arjona R, Daza L (2005) J Power Sources 151:11.
[2] Haryanto A, Fernando S, Murali N, Adhikari S (2005) Energy & Fuels 19:2098.
[3] de Lima SM, da Cruz IO, Jacobs G, Davis BH, Mattos LV, Noronha FB (2008) J Catal 257:356.
[4] Birot A, Epron F, Descorme C, Duprez D (2008) Appl Catal B: Environ 79:17.
[5] Cai W, Wang F, Zhan E, Van Veen AC, Mirodatos C, Shen W (2008) J Catal 257:96.
[6] Davda RR, Shabaker JW, Huber GW, Cortright RD, Dumesic JA (2003) Appl Catal B: Environ 43:13.
[7] Li S, Li M, Zhang C, Wang S, Ma X, Gong J (2012) Int J Hydrogen Energy 37:2940.
[8] Wang F, Li Y, Cai W, Zhan E, Mu X, Shen W (2009) Catal Today 146:31.
[9] Zhang Z, Verykios XE (1996) Appl Catal A: General 138:109.
[10] Al-Fatish ASA, Ibrahim AA, Fakeeha AH, Soliman MA, Siddiqui MRH, Abasaeed AE (2009) Appl Catal A: General 364:150.
[11] Li Z, Hu X, Zhang L, Liu S, Lu G (2012) Appl Catal A: General 417-418:281.
[12] Centi G, Perathoner S (2009) Catal Today 148:191.
[13] Gonzalez-DelaCruz VM, Holgado JP, Pereníguez R, Caballero A (2008) J Catal 257:307.
[14] Christensen KO, Chen D, Lødeng R, Holmen A (2006) Appl Catal A: Gen 314:9.
[15] Chen D, Christensen KO, Ochoa-Fernandez E, Yu Z, Tøtdal B, Latorre N, Monzòn A, Holmen A (2005) J Catal 229:82.
[16] Davda RR, Shabaker JW, Huber GW, Cortright RD, Dumesic JA (2005) Appl Catal B: Environ 56:171.
[17] Qihai L, Zili L, Xinhua Z, Cuijin L, Jiao D (2011) J Rare Earths 29:872.
[18] Remón J, Medrano JA, Bimbela F, García L, Arauzo J (2013) Appl Catal B: Environ 132-133:433.
[19] Fierro V, Akdim O, Mirodatos C (2003) Green Chem 5:20.
[20] Calles JA, Carrero A, Vizcaíno AJ (2009) Microp Mesop Mater 119:200.
[21] Tuza PV, Manfro RL, Ribeiro NFP, Souza MMVM (2013) Renewable Energy 50:408.
[22] Nichele V, Signoretto M, Menegazzo F, Gallo A, Dal Santo V, Cruciani G, Cerrato G (2012) Appl Catal B: Environ 111-112:225.
[23] Rossetti I, Biffi C, Bianchi CL, Nichele V, Signoretto M, Menegazzo F, Finocchio E, Ramis G, Di Michele A (2012) Appl Catal B: Environ 117-118:384.
[24] Rossetti I, Gallo A, Dal Santo V, Bianchi CL, Nichele V, Signoretto M, Finocchio E, Ramis G, Di Michele A (2013) ChemCatChem 5:294.
[25] Rossetti I, Lasso J, Nichele V, Signoretto M, Finocchio E, Ramis G, Di Michele A (2014) Appl Catal B: Environ 150-151:257.
[26] Nichele V, Signoretto M, Pinna F, Menegazzo F, Rossetti I, Cruciani G, Cerrato G, Di Michele A (2014) Appl Catal B: Environ 150-151:12.
[27] Zane F, Melada S, Signoretto M, Pinna F (2006) Appl Catal A: General 299:137.
[28] Asencios YJO, Assaf EM (2013) Fuel Process Technol 106:247.
[29] Bellido JDA, Assaf EM (2008) J Power Sources 177:24.
[30] Zhang L, Lin J, Chen Y (1992) J Chem Soc Faraday Trans 88(14):2075.
[31] Yan QG, Weng WZ, Wan HL, Toghiani H, Toghiani RK, Pittman CU, Jr (2003) Appl Catal A: General 239:43.
[32] Song YQ, He DH, Xu BQ (2008) Appl Catal A: General 337:19.
[33] García V, Fernández JJ, Ruíz W, Mondragón F, Moreno A (2009) Catal Commun 11:240.
[34] Bellido JDA, De Souza JE, M'Peko JC, Assaf EM (2009) Appl Catal A: General 358:215.
[35] Bellido JDA, Assaf EM (2009) Appl Catal A: General 352:179.
[36] Fabris S, Paxton AT, Finnis MW (2002) Acta Mater 50:5171.
[37] Vizcaino AJ, Carrero A, Calles JA (2007) Int J Hydrogen Energy 32:1450.
[38] Zhang L, Liu J, Li W, Guo C, J. Zhang J (2009) J Natural Gas Chem 18:55.

[39] Pérez-Hernández R, Mondragón Galicia G, Mendova Anaya D, Palacios J, Angeles-Chavez C, Arenas-Alatorre J (2008) Int J Hydrogen Energy 33:4569.
[40] Maia TA, Bellido JDA, Assaf EM, Assaf JM (2007) Quim Nova 30:339.
[41] López P, Mondragón-Galicia G, Espinosa-Pesqueira ME, Mendoza-Anaya D, Fernández ME, Gómez-Cortés A, Bonifacio J, Martínez-Barrera G, Pérez-Hernández R (2012) Int J Hydrogen Energy 37:9018.
[42] Nichele V, Signoretto M, Menegazzo F, Rossetti I, Cruciani G (2014) Int J Hydrogen Energy 39:4252.
[43] Rossetti I, Lasso J, Finocchio E, Ramis G, Nichele V, Signoretto M, Di Michele A (2014) Appl Catal A: General 477:42.